Experimental and Numerical Investigations of Subcooled Boiling Heat Transfer in a Small-Diameter Tube

Shibahara, Makoto
Liu, Qiusheng
Hata, Koichi
Fukuda, Katsuya

EXPERIMENTAL AND NUMERICAL INVESTIGATIONS OF SUBCOOLED BOILING HEAT TRANSFER IN A SMALL-DIAMETER TUBE

Makoto Shibahara[1]
Graduate School of Maritime Sciences,
Kobe University, Kobe, Hyogo, Japan
sibahara@maritime.kobe-u.ac.jp

Qiusheng Liu
Graduate School of Maritime Sciences,
Kobe University, Kobe, Hyogo, Japan
qsliu@maritime.kobe-u.ac.jp

Koichi Hata
Graduate School of Maritime Sciences,
Kobe University, Kobe, Hyogo, Japan
hatako1@people.kobe-u.ac.jp

Katsuya Fukuda
Graduate School of Maritime Sciences,
Kobe University, Kobe, Hyogo, Japan
fukudak@kobe-u.ac.jp

ABSTRACT

The boiling heat transfer for subcooled water flowing in a small-diameter tube was investigated experimentally and numerically. In the experiment, a platinum tube was used as an experimental tube (d = 1.0-2.0 mm) to conduct joule heating by direct current. The heat generation rate of the tube was controlled with an exponential function. The numerical simulation of boiling heat transfer for subcooled water flowing in the small-diameter tube was conducted using the commercial computational fluid

[1] Makoto Shibahara, Graduate School of Maritime Sciences, Kobe University, Kobe, Hyogo, Japan

dynamics (CFD), PHOENICS ver. 2013. The small-diameter tube was modeled in the simulation. As the boundary condition, the measured heat flux was given at the inner wall. The inlet temperature ranged from 302 to 312 K. The flow velocities of d= 1.0 mm and d = 2.0 mm were 9.29 m/s and 2.34 m/s, respectively. The three-dimensional analysis was carried out from non-boiling to the critical heat flux. Governing equations were discretized using the finite volume method in the PHOENICS. The SIMPLE method was applied in the numerical simulation. For modeling boiling phenomena in the tube, the Eulerian-Eulerian two-fluid model was adopted using the interphase slip algorithm of PHOENICS. The surface temperature difference increased as the heat flux increased in the experiment. The numerical simulation predicted the experimental data well. When the heat flux of the experiment was reached to the CHF point, the predicted value of the heat transfer coefficient was approximately 3.5 % lower than that of the experiment.

1 Introduction

The Knowledge of boiling heat transfer characteristics for subcooled water in tubes is important for safety assessments of waste heat recovery systems from marine transportations, electric cooling systems of electric propulsion ships and plasma-facing components [1, 2, 3]. For thermal designs in these applications, high heat transfer coefficients for subcooled water have been required using miniature channels and boiling heat transfer with nanofluids [4,5].

When the heat flux exceeds a maximum value in liquid, vapor covered on the heated surface. After that, the heated wall temperature increased rapidly and physical burn out occurs because the heat transfer coefficient decreases by the vapor. Therefore, the maximum heat flux is defined as the critical heat flux (CHF). In order to clarify CHF

characteristics in a narrow channel, their mechanisms were investigated through several types of research such as flow boiling experiments and numerical analyses.

Mudawar and Bowers [6] measured ultra-high CHFs for subcooled water flowing in micro and miniature tubes at various subcooling and mass velocities. Hall and Mudawar [7] obtained correlations of CHFs on high heat flux and high mass flux conditions based on the experimental data of Mudawar and Bowers [6]. Hata and Masuzaki [8] conducted flow boiling experiments for subcooled water. They evaluated the effects of heat input signals such as a step, a lamp and an exponential function on the CHF for subcooled water flowing in conventional tubes. Celata et al. [9] suggested a mechanistic model; The CHF occurs when a liquid sublayer covered a vapor clot is wasted by a heated wall. This assumption was that the vapor clot was created after coalescing vapor bubbles into large units. Then, they validated this model with their CHF data [10, 11].

Shibahara et al. [12] investigated the effects of flow velocities, heat generation rates, subcooling, a ratio of heated length to inner diameter, and system pressures on the CHF. It was found that the CHF is dependent on outlet pressures, subcooling, and flow velocities. The authors also reported that CHF values in steady-state were higher than those of the mechanistic model at low outlet subcooling [13]. Therefore, an empirical correlation of CHF was suggested [14]. However, single-phase and boiling heat transfer for subcooled water were not discussed numerically. Shibahara et al. also investigated the effect of thermal boundary thickness on the heat transfer coefficient for single-phase flow using the commercial CFD, PHOENICS ver.2013 [15]. Although the

numerical predicted way of the CHF was proposed [16, 17], it was not enough to discuss the boiling region about the CHF in the small-diameter tube.

In this study, the boiling heat transfer for subcooled water flowing in a small-diameter tube was investigated experimentally and numerically. This research is aimed to obtain fundamental data from non-boiling to the CHF in a small-diameter tube. Moreover, it is to clarify the void fraction at the CHF using the Eulerian-Eulerian two-fluid model comparing the experimental data and the numerical simulation.

2 Flow Boiling Experiment

2.1 Experimental Method

The experimental apparatus consisted of a circulating pump, a preheater, a Coriolis mass flow meter, a pressurizer, a cooler, and a test section, as shown in Fig.1. The distilled and deionized water was circulated by the pump. The test loop was pressured by the pressurizer. In this study, a vertical platinum tube was used as the experimental tube because the electrical properties of platinum are more stable than those of stainless steel. The electric circuit consisted of the DC power supply, a standard resistor, a double bridge circuit including the platinum tube [18]. The electric resistance of the platinum tube was measured by the double bridge circuit.

In this experiment, the platinum tube was heated by the DC power supply as resistive heating. The average temperature of the tube, T_a, was measured by the platinum resistance thermometry. A value of T_a can be expressed as $R_T = R_0(1+c_1T_a-c_2T_a^2)$, where R_T is the electrical resistance of the platinum tube. The above

relationship between R_T and T_a was calibrated before the experiment. The value of R_T was measured by the unbalance voltage of the double bridge circuit [18]. The heat flux can be expressed by the following equation:

$$q = \frac{V}{A}\left(\dot{Q} - \rho_h c_h \frac{dT_a}{dt}\right) \tag{1}$$

where, V, A, $\dot{Q}$, ρ_h, c_h, and t denote, respectively, the volume of the tube, the inner surface area of the tube, the exponential heat input, density of tube, specific heat of tube, and time.

Inner surface temperatures of the experimental tube can be calculated using the following heat conduction equation.

$$\frac{d^2T}{dr^2} + \frac{1}{r}\frac{dT}{dr} + \frac{\dot{Q}}{\lambda} = 0 \tag{2}$$

$$T(r) = -\frac{\dot{Q}r^2}{4\lambda} + \frac{\dot{Q}r_o^2}{2\lambda} ln\, r + C \tag{3}$$

$$T_a = \frac{1}{\pi(r_o^2 - r_i^2)}\int_{r_i}^{r_o} 2\pi r T(r) dr \tag{4}$$

$$T_s = T(r_i) = T_a - \frac{qr_i}{4(r_o^2 - r_i^2)^2\lambda} \times \left[4r_o^2\left\{r_o^2\left(\ln r_o - \frac{1}{2}\right) - r_i^2\left(\ln r_i - \frac{1}{2}\right)\right\} - \left(r_o^4 - r_i^4\right)\right] - \frac{qr_i}{2(r_o^2 - r_i^2)\lambda}\left(r_i^2 - 2r_o^2 ln r_i\right) \tag{5}$$

$$C = T_a - \frac{qr_i}{4(r_o^2 - r_i^2)^2\lambda} \times \left[4r_o^2\left\{r_o^2\left(\ln r_o - \frac{1}{2}\right) - r_i^2\left(\ln r_i - \frac{1}{2}\right)\right\} - \left(r_o^4 - r_i^4\right)\right] \tag{6}$$

The measurement uncertainties of $\dot{Q}$, q, T_a, T_s, T_l, P, G, L, d and d_o were calculated by the ANSI/ASME PTC 19.1-1985 [19] as shown in Table 1.

2.2 Experimental Conditions

Experimental conditions are summarized as shown in Table 2. The exponential heat input due to Joule heating was defined as $Q_0 e^{(t/\tau)}$, where, τ is the e-folding time. Since the electric power of heat input was controlled by the longer e-folding time as shown in Table 2, the heat generation rate of the tube increased gradually. Since convective heat transfer coefficients approach asymptotic values when the increase of heat generation rate is slow [4, 18], the heat transfer process can be assumed to be in quasi-steady state.

3 Numerical Simulation

3.1 Physical Model of Numerical Simulation

The physical model of the numerical simulation is shown in Fig. 2. The experimental tube was divided into the heated and non-heated sections. In the heated section, a heat flux measured by the experiment was uniformly provided from the tube wall. The working fluid was subcooled water, and it flowed upward. Since the computational geometry was developed by the cylindrical polar coordinate, the radius, circumferential and axial directions were defined as r, θ, and z, respectively.

3.2 Numerical Method

The commercial CFD code, PHOENICS ver. 2013 was used in this study. The Eulerian-equation solver of PHOENICS is based on the interphase slip algorithm (IPSA) to solve the coupling pressure, velocity, and volume fraction in the two-phase flow [15]. Governing equations such as continuity, momentum, energy, and transport equations

for k and ε were discretized by the finite volume method (FVM). In the PHOENICS code, the semi-implicit method for pressure linked equations (SIMPLE) was used. The time step was calculated by the Courant Friedrichs–Lewy (CFL) condition. The Lam–Bremhorst (LB) low Reynolds k–ε turbulent model [20] was applied in the numerical simulation. The model constant of the turbulent is shown in Table.3. The LB low Reynolds k–ε turbulent model differs from the standard k-ε turbulent model in that $C_{\varepsilon 1}$ and $C_{\varepsilon 2}$ are multiplied respectively by the dumping function as follows:

$$f_1 = 1 + \left(\frac{0.05}{f_\mu}\right)^3 \tag{7}$$

$$f_2 = 1 - e^{-\mathrm{Re}_t^2} \tag{8}$$

$$f_\mu = (1 - e^{-0.0165\mathrm{Re}_r})^2 \left(1 + \frac{20.5}{\mathrm{Re}_t}\right) \tag{9}$$

$$\mathrm{Re}_t = \frac{k^2}{\varepsilon \nu} \tag{10}$$

$$\mathrm{Re}_r = \frac{k^{1/2} r}{\nu} \tag{11}$$

where, k, ε, ν, and r are the turbulence kinetic energy, the dissipation rate, the kinematic viscosity, and the distance from the wall, respectively.

The heated surface temperature of the tube can be calculated by the following equation:

$$T_s = (1 - \alpha) \frac{q}{\lambda_l} \frac{\Delta r}{2} + T_{cell} \tag{12}$$

where, α, q, Δr, λ_l, and T_{cell} denote, respectively, the void fraction, the heat flux, the width of the first mesh in the r direction, the thermal conductivity of liquid and the cell temperature of the computational grid. Since the surface temperature was affected by

Δr, the size of Δr was determined by the comparison between the numerical result and the experimental data. Based on the result of sensitivity analysis for computational grids, the number of the computational grid for r, θ, and z were 20, 12, and 150, respectively.

Figure 3 shows the typical temperature profile of T_{cell} with non-dimensionless time (t/τ) for the flow direction. The thermal boundary layer was thicker at the downstream because of convection heat transfer, and it was developed with an increase of t/τ. Moreover, since T_{cell} reached the saturated temperature at the downstream, these temperature profiles showed a constant value.

Since the exponential heat flux was provided from the DC power source in the experiment, the measured heat flux was given as the wall boundary condition. The non-slip condition was also used at the inner wall in the numerical simulation.

In order to model the subcooled boiling, the Eulerian-Eulerian two-fluid model was applied in the numerical simulation. This model consists of various source terms such as the interfacial drag force, lift force, and pressure and virtual mass force. Table 4 shows the coefficients of the interfacial forces based on the PHOENICS manual [15] and open literature [21, 22].

4 Results and Discussion

The numerical simulation was compared with the experimental data of d = 1.0 mm. Figure 4 shows the relationship between the heat flux and the surface temperature difference, ΔT_l, (= $T_s - T_l$) at the flow velocity of 9.29 m/s. The inlet temperature and the inlet pressure are 302 K and 391 kPa, respectively. The open circle and the solid line are

the experimental data and the numerical result, respectively. For the comparison between the numerical result and the experimental data, the numerical result was in good agreement with the experimental data. As shown in Fig.4, the surface temperature difference increased until the heat flux reached to the surface temperature difference of approximately 100 K. For lower surface temperature differences, the relationship between the heat flux and the surface temperature difference shows a linear trend because of single-phase flow. Thus, the heat transfer coefficient was almost constant value since the flow profile is a single-phase flow, where the convective heat transfer becomes dominant. For comparison, the dashed line shows the values of the emperical correlation suggested by Adams et al. [23], as shown in Fig.4. In the non-boiling region, the result of numerical simulation was in good agreement with the values of their correlation within 10 %. When the heat flux was up to approximately 1×10^7 W/m^2, the boiling initiation started. It was found that the surface temperature difference remained around 100 K because of the subcooled boiling, and the CHF value was 20.7×10^6 W/m^2.

Figure 5 indicated the averaged void fraction, surface temperature and bulk temperature for the inner diameter of 1.0 mm in the numerical simulation. While the surface temperature remained around 443 K because of boiling initiation, the bulk temperature increased with an increase in heat flux. Consequently, the surface temperature difference, $\Delta T_l=T_s-T_l$, decreased with an increase in averaged void fraction.

Figure 6 shows the relationship between the heat transfer coefficient and the heat flux at the flow velocity of 2.34 m/s for the inner diameter of 2.0 mm. The inlet temperature and the inlet pressure are 312 K and 548 kPa, respectively. The open

symbol depicts the experimental data, and the solid and dashed lines show the predicted value from the numerical simulation. The heat transfer coefficient was calculated using the heat flux and the temperature difference between the averaged surface temperature and the averaged bulk-liquid temperature. As the heat flux increased, the heat transfer coefficient increased because of nucleate boiling. The numerical simulation predicted the experimental data at the Δr of 9 μm. When the heat flux was reached to the CHF point, the predicted value of the heat transfer coefficient was approximately 3.5 % lower than that of the experiment. As shown in Fig.6, the averaged void fraction increased with increasing the heat flux. When the averaged void fraction is approximately 0.4, the measured heat flux would be reached to the CHF in the experiment.

Figure 7 shows the local void fraction at the CHF for the inner diameter of 2.0 mm. The inlet flow velocity and the inlet temperature were 2.34 m/s and 312 K, respectively. Since the surface boiling occurred on the heated wall, higher void fraction generated at the outlet region of the heated section as shown in Fig.7.

5 Conclusions

The boiling heat transfer for subcooled water flowing in a small-diameter tube was investigated numerically and experimentally. The numerical simulation for subcooled water in the tube was conducted using the commercial CFD code, PHOENICS. The numerical result showed that the surface temperature differences for the inner diameter of 1.0 mm were in agreement with the experimental data from non-boiling to

subcooled boiling. While the surface temperature remained because of boiling initiation, the bulk temperature increased with an increase in heat flux. Consequently, the surface temperature difference decreased with an increase in averaged void fraction.

The heat transfer coefficient in the numerical simulation was compared with the experimental data for the inner diameter of 2.0 mm. The numerical simulation predicted the experimental data at the Δr of 9 μm. When the heat flux of the experiment was reached to the CHF point, the predicted value of the heat transfer coefficient was approximately 3.5 % lower than that of the experiment. Moreover, when the heat flux was reached to the CHF, it was found that a higher void fraction generated at the outlet of the heated tube since the surface boiling occurred near the heated wall.

ACKNOWLEDGMENT

This work was partially supported by the JSPS KAKENHI Grant Number (JP16K18322, JP15K05828). This work was partially performed with the support and under the auspices of NIFS Collaboration Research program (NIFS18KEMF110, NIFS19KEMF138).

FUNDING

JSPS KAKENHI, Grant Number (JP16K18322, JP15K05828)

NIFS Collaboration Research program (NIFS18KEMF110, NIFS19KEMF138)

NOMENCLATURE

A	inner surface area of the platinum tube, (m^2)
C_D	coefficient of interfacial drag force
C_L	coefficient of lift force
C_p	coefficient of pressure force
C_{vm}	coefficient of virtual mass force
$C_{\varepsilon 1}$, $C_{\varepsilon 2}$	constant of transportation equation for ε
C_μ	constant of eddy viscosity in k-ε model
c_1, c_2	constant
c_h	specific heat of the platinum tube, (J/kgK)
d	inner diameter of the platinum tube, (m)
G	mass flow rate, (kg/min)
h	$=q/\Delta T_l$, heat transfer coefficient, (W/m^2)
k	turbulence kinetic energy, (m^2/s^2)
L	heated length, (m)
P	pressure, (kPa)
Q	heat transfer rate, (W)
Q_0	initial exponential heat input, (W/m^3)
$\dot{Q}$	$= Q_0 \exp(t/\tau)$, heat input per unit volume, (W/m^3)

q	heat flux, (W/m^2)
Re	$=\rho ud/\mu$, Reynolds number
R_0	electrical resistance at 0 °C, (Ω)
R_T	electrical resistance of the platinum tube, (Ω)
r	radius of the platinum tube, (m)
Δr	width of the first mesh in the r direction, (μm)
T	temperature, (K)
T_a	average temperature of the platinum tube, (K)
T_c	temperature of K-type sheathed thermocouple, (^oC)
t	time, (s)
ΔT_l	$= T_s - T_l$, surface temperature difference, (K)
u	flow velocity, (m/s)
V	volume of the platinum tube, (m^3)
z	Axial direction, (m)

Greek symbols

α	void fraction
λ	thermal conductivity, (W/mK)
ε	dissipation rate, (m^2/s^3)
ν	kinematic viscosity, (m^2/s)

ρ_h	density, (kg/m^3)
τ	$=\int_0^t Q(t)dt / Q(t)$, e-folding time, (s)
σ_k	Effective Prandtl number for *k*
σ_ε	Effective Prandtl number for ε
θ	circumference direction, (rad)

Subscripts

cell	cell temperature
e	entrance
ex	exit
i	Inner
in	Inlet
l	liquid
o	outer
out	outlet
r	radial direction
s	surface
T	turbulence

REFERENCES

[1] Shibahara, M., Liu, Q.S, Fukuda, K., 2016, "Heat Transfer Characteristics of D-mannitol as a Phase Change Material for a Medium Thermal Energy System," Heat and Mass Transfer, **52** (9), pp.1993-2004.
[2] Shibahara, M., Fukuda, K., Liu, Q.S., Hata, K., Masuzaki, S., 2018, "Boiling Incipience of Subcooled Water Flowing in a Narrow Tube Using Wavelet Analysis," Appl. Therm. Eng., **132** (5), pp.595-604.
[3] Mudawar, I., 2011, "Two-phase Microchannel Heat Sinks: Theory, Applications, and Limitations," J Electron Packaging, **133** (4), p. 41002.
[4] Shibahara, M., Fukuda, K., Liu, Q.S., Hata, K., 2017, "Single-phase Convective Heat Transfer in a Circular Minichannel with Unsteady Thermal Loads," Heat Transf. Res., **53**(9), pp.2999-3012.
[5] Ali, H.M., Generous, M.M., Ahmad, F., Irfan, M., 2017, "Experimental investigation of nucleate pool boiling heat transfer enhancement of TiO_2-water based nanofluids," Appl. Therm. Eng., **113**(25), pp.1146-1151.
[6] Mudawar, I., Bowers, M.B., 1999, "Ultra-high Critical Heat Flux (CHF) for Subcooled Water Flow Boiling-I: CHF Data and Parametric Effects for Small Diameter Tubes," Int. J. Heat Mass Transfer, **42** (8), pp.1405–1428.
[7] Hall, D.D., Mudawar, I., 1999, "Ultra-high Critical Heat Flux (CHF) for Subcooled Water Flow Boiling-II: High-CHF Database and Design Equations," Int. J. Heat Mass Transfer **42** (8), pp.1429–1456.
[8] Hata, K., Masuzaki, S., 2010, "Subcooled Boiling Heat Transfer for Turbulent Flow of Water in a Short Vertical Tube," J Heat Trans, **132**, pp.11501-1-11501–11.
[9] Celata, G.P., Cumo, M., Mariani, A., Simoncini, M., Zummo, G., 1994, "Rationalization the Prediction of Existing Mechanistic Models for the Prediction of Water Subcooled Flow Boiling Critical Heat Flux," Int. J. Heat Mass Transfer, **37** (Suppl.1), pp.347–360.
[10] Celata, G.P., Cumo, M., Mariani, A., 1992, "Subcooled Water Flow Boiling CHF with Very High Heat Fluxes," Rev. Gen. Therm., **31**(362), pp. 106–114.
[11] Celata, G.P., Cumo, M., Mariani, A., 1993, "Burnout in Highly Subcooled Flow Boiling in Small Diameter Tubes," Int. J. Heat Mass Transf, **36**, pp. 1269–1285.
[12] Shibahara, M., Fukuda, K., Liu, Q.S., Hata, K., Nakamura, Y., Muroga, T., Tokitani, M., Noto, H., 2016, "Transient Critical Heat Flux for Subcooled Boiling of Water Flowing Upward through a Vertical Small-diameter Tube with Exponentially Increasing Heat Inputs," J. Therm. Sci. Technol., **11**(3), pp. 16-00377.
[13] Shibahara, M., Fukuda, K., Liu, Q.S, Hata, K., 2017, "Steady and Transient Critical Heat Flux for Subcooled Water in a Mini Channel," Int. J. Heat Mass Transfer, **104**, pp.267-275.
[14] Shibahara, M., Fukuda, K., Liu, Q.S., Hata, K., 2017, "Correlation of High Critical Heat Flux During Flow Boiling for Water in a Small Tube at Various Subcooled Conditions," Int. Commun. Heat Mass Transfer, **82**, pp.74-80.
[15] Spalding, B., 2008, *THE PHOENICS ENCYCLOPAEDIA*, Concentration Heat and Momentum Limited, UK.

[16] Shibahara, M., Liu, Q.S, Fukuda, K., 2016, “Transient Forced Convection Heat Transfer for Nitrogen Gas Flowing over Plate Heater with Exponentially Increasing Heat Input,” Int. J. Heat Mass Transfer, **95**, pp.405-415.
[17] Shibahara, M., Fukuda, K., Liu, Q.S., Hata, K., 2018, “Prediction of Forced Convective Heat Transfer and Critical Heat Flux for Subcooled Water Flowing in Miniature Tubes,” Heat and Mass Transfer, **54** (2), pp.501-508.
[18] Shibahara, M., Fukuda, K., Liu, Q.S., Hata, K., 2017, “Steady and transient forced convection heat transfer for water flowing in small tubes with exponentially increasing heat inputs,” Heat and Mass Transfer, **53**, pp.787-797.
[19] ANSI/ASME PTC 19.1-1985, *Measurement Uncertainty, Supplement on Instruments and Apparatus*, *Part 1*, translated by JSME, 1987. ISBN: 978-4-88-898043-2
[20] Lam, C.K.G., Bremhorst, K., 1981, “A Modified Form of the k-ε Model for Predicting Wall Turbulence,” J Fluid Eng, **103** (3), pp.456-460.
[21] Bertodano, M.L.d., Lahey, R.T., Jones, O.C., 1994, “Phase Distribution in Bubbly Two-phase Flow in Vertical Ducts,” Int. J. Multiphase Flow, **5**, pp.805-818.
[22] Anglart, H., Nylund, O., 1996, “CFD Application to Prediction of Void Distribution in Two-phase Bubbly Flows in Rod Bundles,” Nucl. Eng. Des., **163**, pp.81-98.
[23] Adams, T.M., Abdel-Khalik, S.I., Jeter, S.M., Qureshi, Z.H., 1998, “An experimental investigation of single-phase forced convection in microchannels,” Int. J. Heat Mass Transfer **41**, pp.851–857.

Figure Captions List

Fig. 1 Schematic of the experimental apparatus.

Fig. 2 The physical model of the numerical simulation.

Fig. 3 Temperature distributions of T_{cell} at various t/τ.

Fig. 4 The relationship between the heat flux and the surface temperature difference.

Fig. 5 Numerical results of the averaged void fraction, the surface temperature and the bulk temperature for the inner diameter of 1.0 mm.

Fig. 6 The relationship between the heat transfer coefficient and the heat flux for the inner diameter of 2.0 mm.

Fig.7 The local void fraction at the CHF in the numerical simulation for the inner diameter of 2.0 mm.

Table Caption List

Table 1 The measurement uncertainties in the experiment

Table 2 Experimental conditions

Table 3 Turbulence model constants

Table 4 Coefficients of the interfacial forces

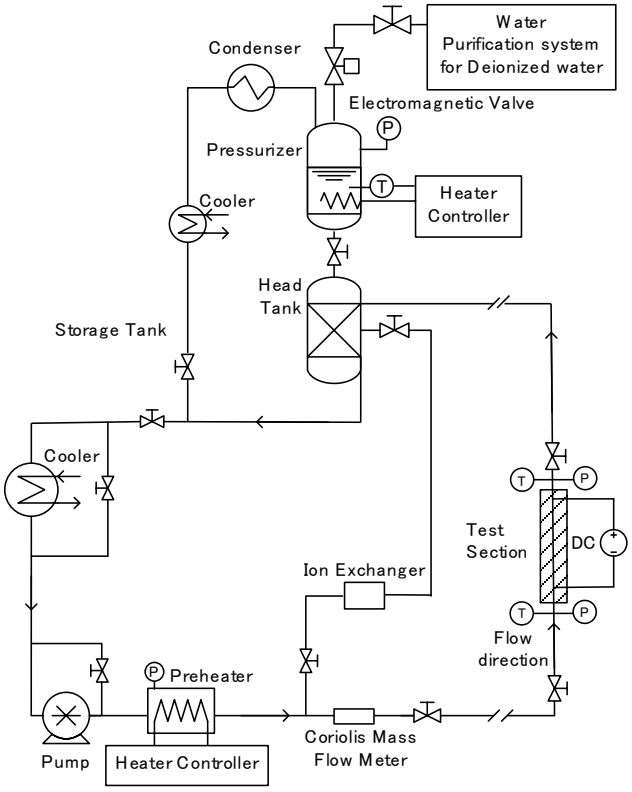

Fig.1 Schematic of the experimental apparatus.

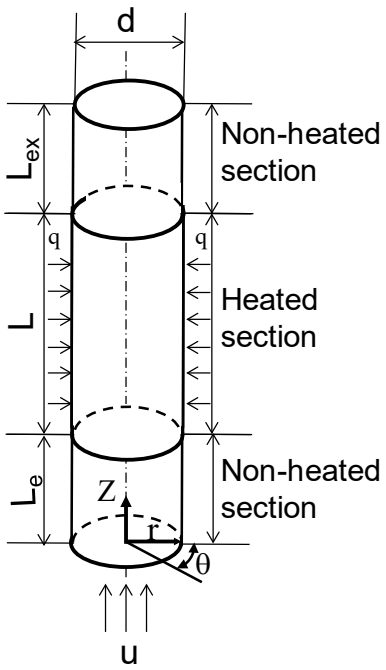

Fig. 2 The physical model of the numerical simulation.

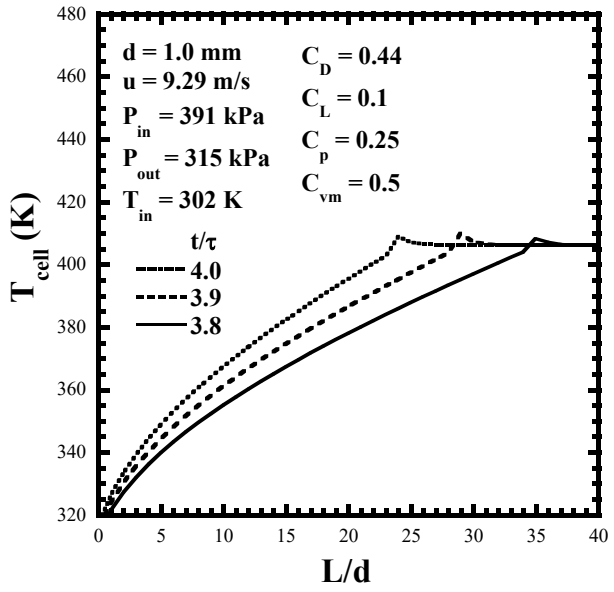

Fig. 3 Temperature distributions of T_{cell} at various t/τ.

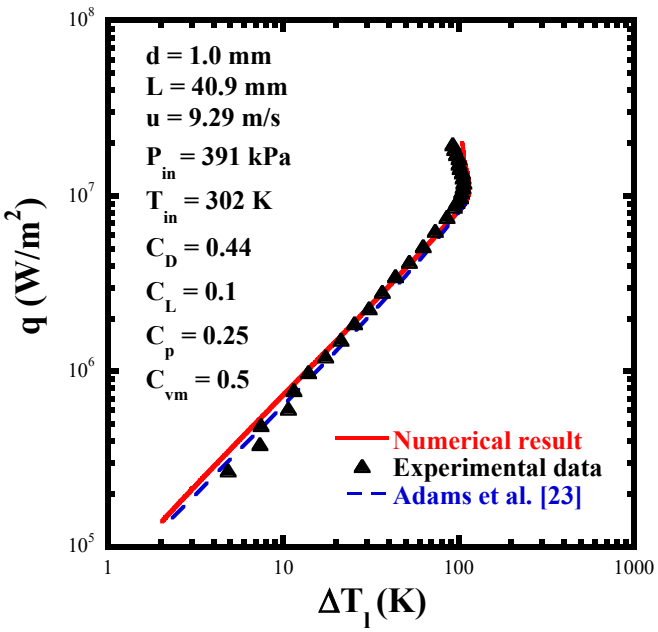

Fig. 4 The relationship between the heat flux and the surface temperature difference.

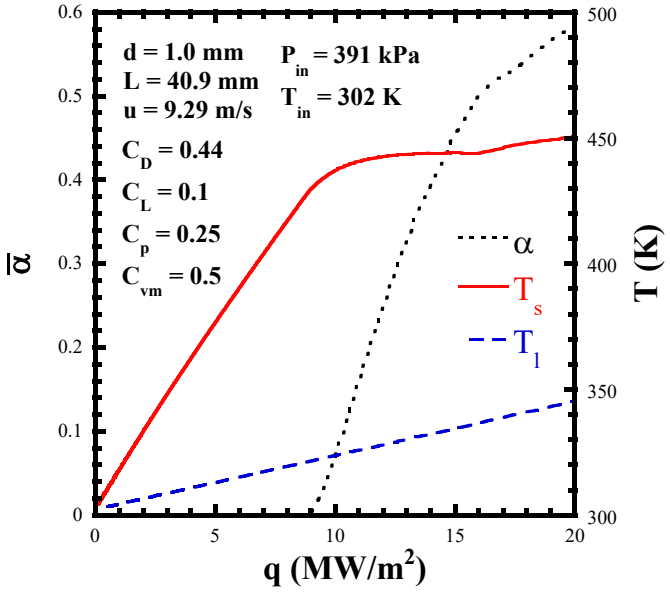

Fig. 5 Numerical results of the averaged void fraction, the surface temperature and the bulk temperature for the inner diameter of 1.0 mm.

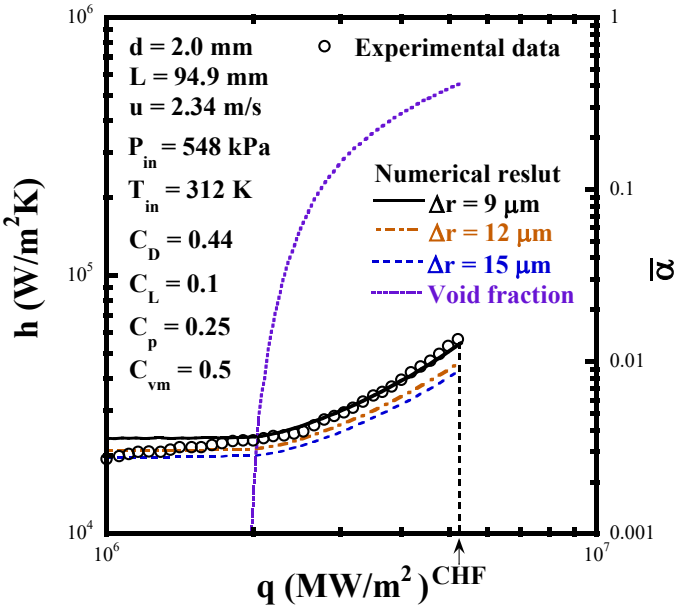

Fig. 6 The relationship between the heat transfer coefficient and the heat flux for the inner diameter of 2.0 mm.

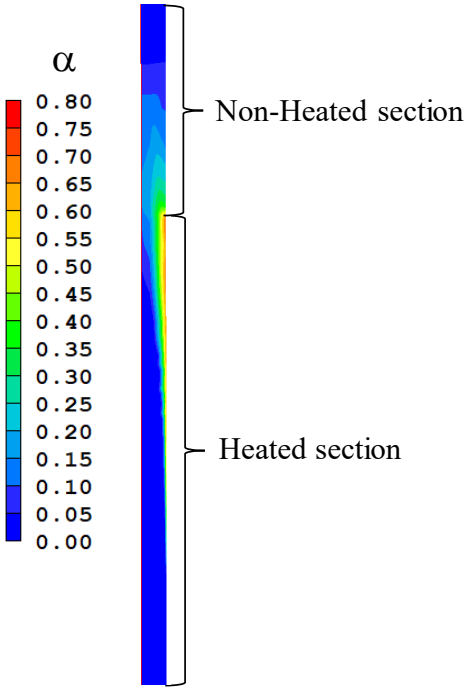

Fig.7 The local void fraction at the CHF in the numerical simulation for the inner diameter of 2.0 mm.

Table 1 The measurement uncertainties in the experiment

Heat generation rate ($\dot{Q}$)	±2.0%
Heat flux (q)	±2.4%
Average temperature of the platinum tube (T_a)	±2.8%
Surface temperature of the platinum tube (T_s)	±2.8%
Thermocouple (T_l)	±0.65K
Pressure gauge (P)	±2.6 kPa
Coriolis Mass flow meter (G)	±0.001 kg/min
Heated length (L)	±0.48 mm
Inner and outer diameter (d, d_0)	±0.015 mm

Table 2 Experimental conditions

Inner diameter	1.0 mm	2.0 mm
Outer diameter	1.8 mm	3.0 mm
Heated length	40.9 mm	94.9 mm
e-folding time	18.4 s	13.4 s
Flow velocity	9.29 m/s	2.34 m/s
Inlet temperature	302 K	312 K
Inlet pressure	391 kPa	548 kPa

Table 3 Turbulence model constants [15, 20]

σ_k	σ_ε	σ_t	$C_{\varepsilon 1}$	$C_{\varepsilon 2}$	C_μ
1	1.3	0.9	1.44	1.92	0.09

Table 4 Coefficients of the interfacial forces [15,21,22]

C_D	C_L	C_p	C_{vm}
0.44	0.1	0.25	0.5